Available online at www.CivileJournal.org

Civil Engineering Journal

Vol. 4, No. 7, July, 2018

An Analytical Method for Crack Detection of Beams with Uncertain Boundary Conditions by a Concentrated Test Mass

Seyed Milad Mohtasebi [a], Naser Khaji [b*]

[a] *Faculty of Civil and Environmental Engineering, Tarbiat Modares university, Tehran, Iran.*

[b] *Professor, Faculty of Civil and Environmental Engineering, Tarbiat Modares university, Tehran, Iran.*

Received 28 May 2018; Accepted 20 July 2018

Abstract

The aim of this study is to introduce a method for crack detection and simultaneously assessing boundary conditions in beams. This study suggests a method based on the effect of a concentrated test mass on the natural frequency that is defined as a stationary mass, which can be located in different positions of the beam and cannot be separated from the beam. Timoshenko beam theory is used to calculate the frequencies. In this method, a beam with the desired number of cracks is modeled. The beam is divided into separated parts at crack section, which are joined together by elastic weightless torsion springs, to avoid non-linearity effects; it is assumed that the crack is always open. At the first step, equations for a cracked beam are extracted by considering the spring boundary conditions. Then, to verify the equations, numerical finite element model is used. In this way, a new method is also applied to model the torsion springs in supports and it is shown that suggested model is acceptable. Eventually, the obtained responses are evaluated and the sources of errors are identified. To correct the existing errors, a modifying function is suggested. Finally, the inverse problem is solved.

Keywords: Timoshenko Beam Theory; Test Mass; Dynamic Characteristics; Cracked Beam; Spring Boundary Conditions.

1. Introduction

Generally, to ensure lifetime safety of structures, their health should be monitored continuously to enable possible damages detection. Therefore, many studies have been conducted in damage detection so far [1]. Non-destructive testing methods are common in crack detection, but these methods are much expensive in comparison with computational methods. On the other hand, in computational methods (e.g., frequency based methods), experimental data collection from one point may be sufficient, and they have some advantages for components which are not fully accessible [2]. Since cracking effects on the dynamic properties of the structures, crack detection can be done with evaluation of these parameters. In this way, calculations are usually achieved using various numerical [3, 4] or analytical methods [2, 5].

For both numerical and analytical methods, some remarkable parameters such as natural frequencies, coefficient of the stress intensity and mode shapes are studied [6-9]. In Ref. [6], location and depth of the crack are estimated from the intersection of the normalized natural frequency (as a function of location and depth of the crack) and an experimental response. In Ref. [7], by using the strain energy density function, the additional flexibility in vicinity of the crack is evaluated, so a new finite element matrix is used to achieve dynamic response when a harmonic force is applied on a cracked free-free beam. Andreaus and Baragatti [8] considered contact surfaces to model non-propagating cracks for analyzing nonlinear behavior of a cantilevered beam. In this procedure, a sensor and driving load are required for crack

* Corresponding author: nkhaji@modares.ac.ir

http://dx.doi.org/10.28991/cej-03091100

detection. Totally, in numerical methods, more general conditions compared to analytical methods are considered. For instance in Ref. [9], the problem of Euler–Bernoulli cantilever beam theory is solved in a tapered beam which is constrained at one end by translational and rotational springs.

Using of Artificial intelligence methods are common in damage detection. The advantages, limitations and research gaps in this field are discussed in Ref. [20], but solution strategy for crack identification would highly benefit from a closed form solution. Therefore, they provide a combination of a closed form solution for the static analysis of multi-cracked beams and a new algorithm for the damage detection in beams. In fact, the availability of the closed form solution of the problem improves the performance of the algorithm. More importantly, it decreases noise induced by measurements errors and the accuracy of the results [21].

To solve this problem and to describe the dynamic behavior of damaged structures, different analytical methods are employed, where in most of them, boundary conditions are assumed as known parameters. In other words, to solve the problem, the supports were considered as a fixed or simple support. In many cases, the performance of the supports is unknown and are not in good agreement with the considered idealization in simple supported beam and clamped-clamped beam [18]. However, it is not possible to find a precise solution for the problem without studying performance of the supports. Furthermore, in many studies, Euler–Bernoulli beam theory is used which ignores shear deformations.

In 2002, Lele and Maiti [2] suggested a new method to solve the cracked beam problem by Timoshenko beam theory. In this new method, the Timoshenko equation for the cracked beam is expressed for a Cantilever beam with 8^{th}-order determinant. Lin [13] studied this problem for a simple boundary condition and introduced the certain beam equation as a closed-form solution. Khaji *et al.* [14] suggested a new method for crack detection problem of Timoshenko beam with various boundary conditions, which is based on bending vibration measurements. They considered six different boundary conditions. In the present study, these equations are developed for the spring boundary conditions.

In some research works, the effect of the desired number of cracks on the dynamic behavior of structure have been studied. Aydin [12] tried to calculate the frequencies and mode shapes of a Timoshenko beam by an analytical method that beam have certain numbers of cracks under axial load. In Ref. [22], a beam is modelled with an arbitrary number of cracks, and development of crack identification approach in uniform simply supported beams by using a concentrated test mass is presented. The calculation was based on changes in natural frequencies of the cracked beams due to the test mass. Test mass is defined as a stationary mass, which is located in different positions of the beam. In the present study, the proposed method is developed for a beam with uncertain boundary conditions.

According to the presented literature review, crack detection of a beam element involves three different aspects: the first one is the effect of cracks, the second one may be considered as the effect of the boundary conditions, and the third is how to detect location and qualification of cracks when the boundary condition is uncertain. Therefore, in this study, all the aspects are applied to achieve the minimum error, for which all equations are derived from Timoshenko beam theory. For verifying the results, finite element model is used. For numerical simulation of torsional springs in supports, a new method is suggested.

2. Theoretical Approach

Equations of the vibrations for a single span beam of the length *L*, the cross-section area of *A*, and moment of inertia *I*, are as follows [15].

$$k'G\left(\frac{\partial^2 y(x,t)}{\partial x^2}-\frac{\partial \psi(x,t)}{\partial x}\right)-\rho\frac{\partial^2 y(x,t)}{\partial t^2}=0 \tag{1}$$

$$EI\frac{\partial^2 \psi(x,t)}{\partial x^2}+k'GA\left(\frac{\partial y(x,t)}{\partial x}-\psi(x,t)\right)-\rho I\frac{\partial^2 \psi(x,t)}{\partial t^2}=0 \tag{2}$$

Where $y(x,t)$ is a transverse deflection function of the beam and $\psi(x,t)$ is the slope of the deflection curve due to bending; *E*, *G*, and ρ indicate the Young's modulus, the shear modulus, and the material mass density, respectively; k' is the shear coefficient that is introduced to account for the geometry- dependent distribution of the shear stress. The above-mentioned equations can be re-written as follows:

$$y(x,t)=LU(x)\exp(j\omega t) \tag{3}$$

$$\psi(x,t)=\Psi(x)\exp(j\omega t) \tag{4}$$

In which $j=\sqrt{-1}$ and ω shows natural frequencies. $U(x)$ and $\Psi(x)$ are normalized functions of $y(x,t)$ and

$\psi(x,t)$. Solving of these normalized functions are according to the following equations:

$$U(\xi) = A\cosh\beta_1\xi + B\sinh\beta_1\xi + C\cos\beta_2\xi + D\sin\beta_2\xi \tag{5}$$

$$\Psi(\xi) = Am_1\sinh\beta_1\xi + Bm_1\cosh\beta_1\xi + Cm_2\sin\beta_2\xi - Dm_2\cos\beta_2\xi \tag{6}$$

In the above-mentioned equations, *A*, *B*, *C*, and *D* are constant and the following variables are given by:

$$\xi = \frac{x}{L},\ \varsigma = \frac{t}{\sqrt{L}},\ \vartheta = \frac{E}{k'G},\ \mathrm{r} = \frac{I}{AL^2},\ \mathrm{s} = \vartheta\, r,\ \alpha = \frac{\rho A}{EI}L^4\omega^2, a = \frac{\alpha(r+s)}{2},$$
$$b = \alpha(\alpha rs - 1),\ \beta_1 = \left(\sqrt{a^2 - b} - a\right)^{1/2},\ \beta_2 = \left(\sqrt{a^2 - b} + a\right)^{1/2}, m_1 = \frac{\alpha s + \beta_1^2}{\beta_1},\ m_2 = \frac{\alpha s - \beta_2^2}{\beta_2} \tag{7}$$

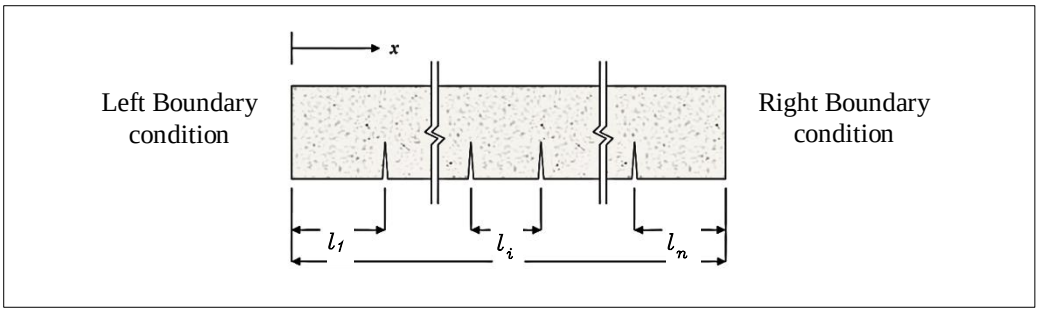

Figure 1. Timoshenko beam with single- sided open crack

According to Figure 1, the beam is divided into *n* parts and the equations of each part are re-written separately, according to the following equations:

$$U_i(\xi - e_{i-1}) = A_i\cosh\beta_1(\xi - e_{i-1}) + B_i\sinh\beta_1(\xi - e_{i-1}) + C_i\cos\beta_2(\xi - e_{i-1}) + D_i\sin\beta_2(\xi - e_{i-1}) \tag{8}$$

$$\Psi_i(\xi - e_{i-1}) = A_i m_1\sinh\beta_1(\xi - e_{i-1}) + B_i m_1\cosh\beta_1(\xi - e_{i-1}) + C_i m_2\sin\beta_2(\xi - e_{i-1}) - D_i m_2\cos\beta_2(\xi - e_{i-1}) \tag{9}$$

In the above-mentioned equations e_i is equal to $\sum_1^i \frac{l_i}{L}$. In addition, U_i and Ψ_i indicate the transverse deflection and the slope of *i*th segment. Moreover, A_i, B_i, C_i and D_i are constant of the *i*th segment.

The conditions for continuity of displacement, moment, and shear force at the crack location are written, respectively, in the following form:

$$U_{i+1}\big|_{\xi=e_i} = U_i\big|_{\xi=e_i} \tag{10}$$

$$\Psi'_{i+1}\big|_{\xi=e_i} = \Psi'_i\big|_{\xi=e_i} \tag{11}$$

$$(U'_{i+1} - \Psi_{i+1})\big|_{\xi=e_i} = (U'_i - \Psi_i)\big|_{\xi=e_i} \tag{12}$$

The cracked section is modeled as a rotational spring to evaluate the effect of the cracks:

$$(U'_{i+1} - U'_i)\big|_{\xi=e_i} = \theta_i\,\Psi'_{i+1}\big|_{\xi=e_i} \tag{13}$$

This equation depends on the extension of the crack and is calculated for a single-sided open crack as below [14]:

$$\theta_i = 6\pi\left(\frac{H}{L}\right)\eta_i^2 f_J(\eta_i) \tag{14}$$

$$\eta_i = \frac{a_i}{H} \tag{15}$$

In the above-mentioned equations, a_i and H are the depth of each crack and the height of the beam, respectively. The function is obtained through the following equation:

$$f_J(\eta_i) = 0.6384 - 1.035\eta_i + 3.7201\eta_i^2 - 5.1773\eta_i^3 + 7.553\eta_i^4 - 7.332\eta_i^5 + 2.4909\eta_i^6 \tag{16}$$

It is worth mentioning, similar equations are proposed for a double-sided open crack.

Using equations 17 and 18, it is possible to re-write the constants of equations in (i+1)th part on the constants of equations in ith part of cracked beam:

$$\mathbf{A}_{(i)} = \begin{bmatrix} A_i \\ B_i \\ C_i \\ D_i \end{bmatrix} \tag{17}$$

$$[\mathbf{A}_{(i+1)}] = [\mathbf{Z}_{(i)}] \cdot [\mathbf{A}_{(i)}] \tag{18}$$

Through a series of mathematical operations, a transformation matrix [Z_i] is calculated [13] as:

$$z_{13,4} = 0,\ z_{12} = \sinh \beta_1 l_i\ ,\ z_{11} = \cosh \beta_1 l_i$$

$$z_{21} = \frac{\beta_2 m_2}{\beta_2 m_1 + \beta_1 m_2}\left(\frac{\beta_1}{\beta_2} m_1 \theta_i \cosh \beta_1 l_i + \frac{\beta_1}{\beta_2}\sinh \beta_1 l_i + \frac{m_1}{m_2}\beta_1 \theta_i \cosh \beta_1 l_i + \frac{m_1}{m_2}\sinh \beta_1 l_i\right)$$

$$z_{22} = \frac{\beta_2 m_2}{\beta_2 m_1 + \beta_1 m_2}\left(\frac{\beta_1}{\beta_2} m_1 \theta_i \sinh \beta_1 l_i + \frac{\beta_1}{\beta_2}\cosh \beta_1 l_i + \frac{m_1}{m_2}\beta_1 \theta_i \sinh \beta_1 l_i + \frac{m_1}{m_2}\cosh \beta_1 l_i\right)$$

$$z_{23} = \frac{\beta_2 m_2}{\beta_2 m_1 + \beta_1 m_2}\theta_i\,(m_2 + \beta_2)\cos \beta_2 l_i$$

$$z_{24} = \frac{\beta_2 m_2}{\beta_2 m_1 + \beta_1 m_2}\theta_i\,(m_2 + \beta_2)\sin \beta_2 l_i$$

$$z_{34} = \sin \beta_2 l_i\ ,\ \ z_{33} = \cos \beta_2 l_i\ ,\ z_{31,2} = 0 \tag{19}$$

$$z_{41} = \frac{\beta_1 m_1}{\beta_2 m_1 + \beta_1 m_2}\theta_i\,(m_1 - \beta_1)\cosh \beta_1 l_i$$

$$z_{42} = \frac{\beta_1 m_1}{\beta_2 m_1 + \beta_1 m_2}\theta_i\,(m_1 - \beta_1)\sinh \beta_1 l_i$$

$$z_{43} = \frac{\beta_1 m_1}{\beta_2 m_1 + \beta_1 m_2}\left(\frac{\beta_2}{\beta_1} m_2 \theta_i \cos \beta_2 l_i - \frac{\beta_2}{\beta_1}\sin \beta_2 l_i - \frac{m_2}{m_1}\beta_2 \theta_i \cos \beta_2 l_i - \frac{m_2}{m_1}\sin \beta_2 l_i\right)$$

$$z_{44} = \frac{\beta_1 m_1}{\beta_2 m_1 + \beta_1 m_2}\left(\frac{\beta_2}{\beta_1} m_2 \theta_i \sin \beta_2 l_i + \frac{\beta_2}{\beta_1}\cos \beta_2 l_i - \frac{m_2}{m_1}\beta_2 \theta_i \sin \beta_2 l_i + \frac{m_2}{m_1}\cos \beta_2 l_i\right)$$

2.1. A Precise Equation for Calculating the Natural Frequency

Consider a beam with a spring boundary condition in both ends as shown in Figure 2. In this figure, K_L and K_R are left and right torsional stiffness coefficients of the beam, respectively. This paper studies a beam with uncertain boundary conditions. The equations are as follows (axial stiffness at supports is considered infinite):

$$U(0) = 0 \tag{20}$$

$$U(1) = 0 \tag{21}$$

$$K_L \frac{\partial U(0)}{\partial x} L - EI \frac{\partial^2 \psi(0)}{\partial x^2} = 0 \tag{22}$$

$$K_R \frac{\partial U(1)}{\partial x} L - EI \frac{\partial^2 \psi(1)}{\partial x^2} = 0 \quad (23)$$

Now, by considering the transformation matrix and equations 20 to 23, presented boundary conditions on both ends of the beam are re-written in the matrix form:

$$[L_{(n)}] \cdot \begin{bmatrix} A_1 \\ B_1 \\ C_1 \\ D_1 \end{bmatrix} = \mathbf{0} \quad (24)$$

The coefficients of the *n*th part of the beam is calculated as the following:

$$[\mathbf{A}_{(n)}] = \left(\prod_{i=1}^{n-1} [\mathbf{Z}_{(i)}] \right) \cdot [\mathbf{A}_{(1)}] \quad (25)$$

Satisfying the four presented boundary conditions leads to a fourth order determinant. Finally, through the following equation, the problem is solved [13].

$$Det[L_{(n)}] = \mathbf{0} \quad (26)$$

The above-mentioned equation is called mother equation. All the parameters of the mother equation are defined as functions of vibration frequency, so vibration frequency can be calculated by solving equation 26.

2.2. Approximate Relationship

A cracked simple beam with a test mass is shown in Figure 2. Frequency calculation can be done in a way that was first provided by the Rayleigh's method. The basic concept of this method is based on the principle of energy conservation law (undamped mode).

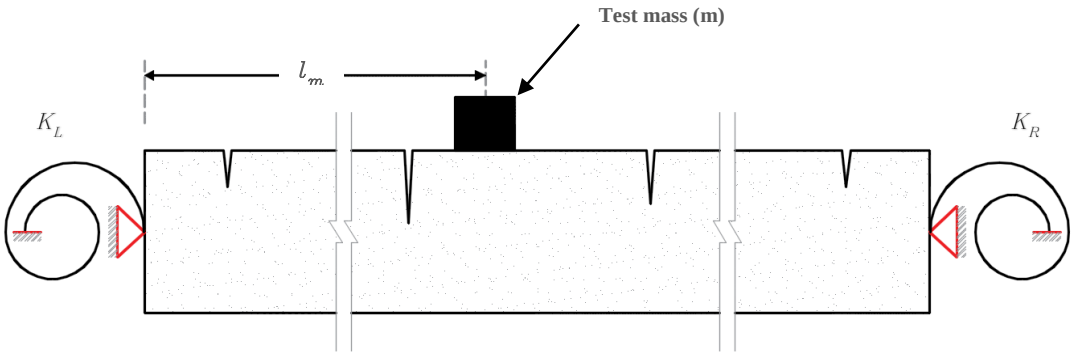

Figure 2. Timoshenko beam with one-sided open cracks and spring boundary condition on both sides with a central mass (test mass)

Expression of the approximate is due to the fact that the natural frequency of the beam is calculated in the presence of the test mass by using mode shapes of cracked beam without the test mass (The mode shapes of the cracked beam with a test mass is considered to be the same as the cracked beam without the mass of the test mass).

Rayleigh calculated the amount of frequency with equalizing the maximum amount of potential energy and the maximum amount of kinetic energy [16] as:

$$U_b = \frac{1}{2} \int_0^L \left[EI \left(\frac{\partial \psi(x,t)}{\partial x} \right)^2 + \kappa' GA \left(\frac{\partial y(x,t)}{\partial x} - \psi(x,t) \right)^2 \right] dx \quad (27)$$

$$T_b = \frac{1}{2} \int_0^L \left[\rho A \left(\frac{\partial y(x,t)}{\partial t} \right)^2 + \rho I \left(\frac{\partial \psi(x,t)}{\partial t} \right)^2 \right] dx \quad (28)$$

The energy generated by the concentrate test mass without considering rotational inertia is obtained from the following equation:

$$T_m = \frac{1}{2} m \left(\frac{\partial y(l_m, t)}{\partial t} \right)^2 \quad (29)$$

Where m is mass of the test mass. If a torsion spring with stiffness of K is placed on the location l_1 of a beam, the potential energy at the torsion spring is equal to:

$$V_{Cr} = \frac{1}{2} K \left(\frac{\partial y_2(l_1, t)}{\partial x} - \frac{\partial y_1(l_1, t)}{\partial x} \right)^2 \quad (30)$$

By changing of variables (equations 3, 4) and normalizing functions and integrals and with considering the hypothesis of equality of kinetic and potential energies, the following equations may be considered [16]:

$$T = \frac{1}{2} \omega^2 \, \mathrm{f}(t)^2 \left[L \int_0^1 \left[\rho A L^2 U(\xi)^2 + \rho I \Psi(\xi)^2 \right] d\xi + m L^2 U(\frac{l_m}{L})^2 \right] \quad (31)$$

$$V = \frac{1}{2} f(t)^2 \left[\int_0^1 \left[\frac{EI}{L} \left(\frac{\partial \Psi(\xi)}{\partial \xi} \right)^2 + \kappa' GAL \left(\frac{\partial U(\xi)}{\partial \xi} - \Psi(\xi) \right)^2 \right] d\xi + \frac{EI\theta}{L} \cdot \left(\frac{\partial \Psi(\frac{l_1}{L})}{\partial \xi} \right)^2 + L^2 K_L \frac{\partial U(0)}{\partial \xi} + L^2 K_R \frac{\partial U(1)}{\partial \xi} \right] \quad (32)$$

The investigation is in the case of undamped mode, and thus the following equation is obtained:

$$T_{\max} = V_{\max} \quad (33)$$

From Equations 31, 32 and 33, the vibration frequency of the beam in the presence of concentrated mass is equal to the following value:

$$\omega^2 = \frac{\left[\int_0^1 \left[\frac{EI}{L} \left(\frac{\partial \Psi(\xi)}{\partial \xi} \right)^2 + \kappa' GAL \left(\frac{\partial U(\xi)}{\partial \xi} - \Psi(\xi) \right)^2 \right] \mathrm{d}\xi + \sum_{i=1}^{n} \frac{EI\theta_i}{L} \left(\frac{\partial \Psi(\xi_i)}{\partial \xi} \right)^2 + L^2 K_L \frac{\partial U(0)}{\partial \xi} + L^2 K_R \frac{\partial U(1)}{\partial \xi} \right]}{\rho AL \int_0^1 \left[L^2 U^2(\xi) + \frac{I}{A} \Psi^2(\xi) \right] \mathrm{d}\xi + m L^2 U^2(\xi_m)} \quad (34)$$

It can be noted that in equation 34, numerator is K^* for this mode shape, while denominator consists of two parts, M^* (due to the mass of the beam) and m^* (due to the mass of the test mass) for this mode shape.

$$\omega^2 = \frac{K^*}{M^* + m^*} \quad (35)$$

$$K^* = \int_0^1 \left[\frac{EI}{L} \left(\frac{\partial \Psi(\xi)}{\partial \xi} \right)^2 + \kappa' GAL \left(\frac{\partial U(\xi)}{\partial \xi} - \Psi(\xi) \right)^2 \right] \mathrm{d}\xi + \sum_{i=1}^{n} \frac{EI\theta_i}{L} \left(\frac{\partial \Psi(\xi_i)}{\partial \xi} \right)^2 + L^2 K_L \frac{\partial U(0)}{\partial \xi} + L^2 K_R \frac{\partial U(1)}{\partial \xi} \quad (36)$$

$$M^* = \rho AL \int_0^1 \left[L^2 U^2(\xi) + \frac{I}{A} \Psi^2(\xi) \right] \mathrm{d}\xi \quad (37)$$

$$m^* = m L^2 U^2(\xi_m) \quad (38)$$

Now, rewrite the following equation to simplify the equation 35.

$$\omega^2 = \frac{M^* \omega_{wm}^2}{M^* + m^*} \quad (39)$$

Where ω_{wm} is equal to the natural frequency of the beam without considering concentrating mass that can be calculated according to Equation 34.

3. The Numerical Model

For assessment and verification of the relationships, results from a finite element model are used to confirm the accuracy of the present forward solutions. The beams with a single-sided transverse cracks of various depths that are located at different locations and spring supports in both sides are studied.

3.1. Cracked Beam Numerical Modeling

The finite element method is employed as a laboratory sample and it should be emphasized that blind application of finite element models may result in considerable errors. So, very small meshes are used to match the numerical and experimental models. For this, the beam is modeled with 8-node isoparametric plane-stress elements and to consider the

singularity of stress at the crack tip, this zone is modeled using an appropriate number of quarter-point singular elements [17].

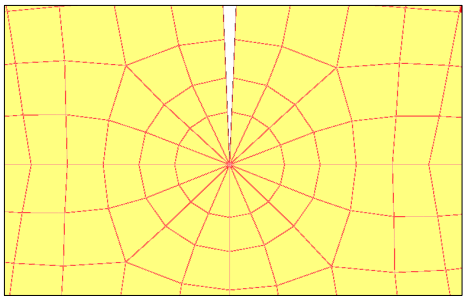

Figure 3. The method of modeling in Ansys software

3.2. Simulation of Beam Boundary Conditions

In supports, elastic conditions is considered. The transferring stiffness in the supports are infinite. As a result, for simplicity, a simply supported beam with torsion springs in both sides is assumed, as shown in Figure 4.

In 2D or 3D finite element model, torsional springs cannot be simulated directly. Therefore, a new method is suggested to model torsional springs and they are simulated by the special arrangement of longitudinal springs, as depicted in Figure 5. The stiffness of the longitudinal springs is calculated from the torsional stiffness of the torsional springs. In each support, the stiffness of longitudinal springs are equal. In these equations, it is assumed that the plane cross-sections remain plane, as shown in Figure 6. The following steps are presented to prove these assumptions:

a) By consideration of the torsional stiffness in the analytical model, the stiffness of the longitudinal springs are calculated from equations 41 and 42 , $M_{L,R}$ is considered as the left and right sides torsional spring moment and other parameters are defined in Figure 4 to 6.

$$\theta_L = \frac{M_L}{K_L} \ , \theta_R = \frac{M_R}{K_R} \tag{40}$$

$$K_R = \sum K_{ri} \times l_i^2 \quad , \quad K_{r1} = ... = K_{ri} = ... = K_{rm} \ , \tag{41}$$

$$K_L = \sum K_{li} \times l_i^2 \quad , \quad K_{l1} = ... = K_{li} = ... = K_{ln} \tag{42}$$

b) In this step, according to the stiffness of longitudinal springs that are calculated in the previous step, finite element model should be created.

c) According to deformations in the mode shapes of the finite element model, forces in longitudinal springs are calculated which produce a moment in each support.

d) In this step, a linear function will be fitted to the deformations of each end side that this function has minimum standard deviation.

e) Nodal displacements at the end sides of the beam are calculated by applying the rotations of previous step on each side, with the assumption that plane cross-sections remain plane.

f) By using of statics relationships, moment in supports can be calculated.

g) It is concluded from the equality of the moment obtained in steps (c) and (f), that the suggested simulation for torsional spring in supports is acceptable.

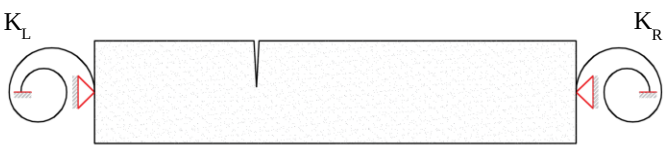

Figure 4. The beam for the analytical model

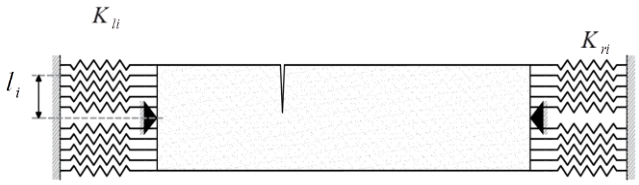

Figure 5. The numerical modeling of the cracked beam in the finite element software

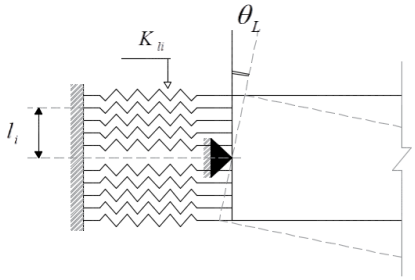

Figure 6. The assumed deformation in the Equations 40, 41 and 42

The considered common geometric data are beam depth H=25 mm and beam thickness B=12.5 mm, the value of the Timoshenko shear coefficient, k' for the rectangular cross-section is taken as 5/6.

Table 1. Evaluating the effect of the presented assumptions in the Equations 40 to 42 by considering the first mode shape of the numerical model ($\frac{L}{H}=5, \eta=0.5, e_1=0.5, \frac{l_m}{L}=0.4, \frac{m}{M}=0.1$)

The obtained responses from the numerical model (step c)					The obtained responses based on the mentioned assumptions (step d)				
l_i	U_{xi}	K_{li}	F_{li}	M_{xi}	l_i	U_{xi}	K_{li}	F_{li}	M_{xi}
0.0125	2.19E-02	3970909091	86863636	1085795.45	0.0125	4.02E-02	3.971E+09	159476943	1993461.8
0.0100	4.27E-02	3970909091	169545905	1695459.05	0.0100	3.21E-02	3.971E+09	127581555	1275815.5
0.0075	2.99E-02	3970909091	118642822	889821.164	0.0075	2.41E-02	3.971E+09	95686166	717646.25
0.0050	2.09E-02	3970909091	83178633	415893.164	0.0050	1.61E-02	3.971E+09	63790777	318953.89
0.0025	3.11E-02	3970909091	123296727	308241.818	0.0025	8.03E-03	3.971E+09	31895389	79738.472
-0.0025	-3.11E-02	3970909091	-123312611	308281.527	-0.0025	-8.03E-03	3.971E+09	-31895389	79738.472
-0.0050	-2.09E-02	3970909091	-82976116	414880.582	-0.0050	-1.61E-02	3.971E+09	-63790777	318953.89
-0.0075	-2.97E-02	3970909091	-118063069	885473.018	-0.0075	-2.41E-02	3.971E+09	-95686166	717646.25
-0.0100	-4.25E-02	3970909091	-168640538	1686405.38	-0.0100	-3.21E-02	3.971E+09	-127581555	1275815.5
-0.0125	-2.18E-02	3970909091	-86478458	1080980.73	-0.0125	-4.02E-02	3.971E+09	-159476943	1993461.8
The total moment in the left support (N.m)				8771231.89	The total moment in the left support (N . m)				8771231.9
Percentage of error					2.28944E-09				

The stated operation is done for three higher modes similar to those obtained in this mode, and the similar results are obtained.

Table 2. Evaluating the effect of the presented assumptions in the Equations 40 to 42 by considering the second, third and fourth mode shapes of the numerical model ($\frac{L}{H}=5, \eta=0.5, e_1=0.5, \frac{l_m}{L}=0.4, \frac{m}{M}=0.1$)

Mode No.	unit	results according to the numerical model (step3)	Results according to the assumption (step6)	Error (%)
2	N.M	12419574	12419574	-
3	N.M	-16206561	-16206561	-
4	N.M	16206561	16953935	-

4. Study of Equations

In this section, accuracy of previous parts are shown. Verification will be done by comparison between results of numerical and analytical methods.

4.1. Torsional Stiffness on Supports

The accuracy of equation 39 should be evaluated by changing the stiffness of torsional springs in both sides. If the frequencies of analytical method were equal to the frequencies of numerical, the suggested method is correct.

Table 3. Comparison between first, second and third frequency of the analytical and numerical model by changing in stiffness of torsional springs in supports $(\frac{L}{H}=5,\eta=0.5,e_1=0.5,\frac{m}{M}=0.1,\frac{l_m}{L}=0.4)$

No.	$k_L/(\frac{EI}{L})$	$k_R/(\frac{EI}{L})$	FEM			TBM			Error (%)		
			F1	F2	F3	F1	F2	F3	F1	F2	F3
1	100	100	4901	14046	21172	4772	13191	19304	-2.628	-6.093	-8.823
2	25	25	4591	13635	21002	4496	12789	19175	-2.063	-6.202	-8.699
3	10	10	4191	13173	20761	4110	12389	19027	-1.940	-5.953	-8.352
5	2	2	3246	12282	19591	3211	11874	18648	-1.071	-3.325	-4.814
7	0.5	0.5	2679	11863	19261	2678	11739	19568	-0.034	-1.044	1.594
8	0	0	2379	11672	19116	2390	11676	19358	0.448	0.032	1.263
9	100	0	3729	12608	20238	3590	11840	18541	-3.712	-6.091	-8.384
10	25	0	3566	12453	20000	3441	11685	18378	-3.485	-6.171	-8.108
11	10	0	3351	12275	19762	3245	11548	18355	-3.152	-5.924	-7.121
12	5	0	3134	12114	19570	3048	11486	18606	-2.735	-5.186	-4.927
13	1	0	2654	11816	19253	2628	11581	19514	-0.980	-1.985	1.355

Table 4. Comparison between first, second and third frequency of the analytical and numerical model by changing in location and characteristics of cracks $(\frac{L}{H}=5,\frac{m}{M}=0.1,\frac{l_m}{L}=0.4)$

No.	$\frac{K_L}{(\frac{EI}{L})}$	$\frac{K_R}{(\frac{EI}{L})}$	number of cracks	First crack		Second crack		Third crack		FEM			TBM			Error (%)		
				e_1	η_1	e_2	η_2	e_3	η_3	F1	F2	F3	F1	F2	F3	F1	F2	F3
1	100	100	1	0.5	0.5	*	*	*	*	4901	14046	21172	4772	13191	19304	2.6	6.1	8.8
2	100	0	1	0.5	0.5	*	*	*	*	3729	12608	20238	3590	11840	18541	3.7	6.1	8.4
3	5	5	1	0.5	0.5	*	*	*	*	3792	12766	19261	3728	12105	18773	1.7	5.2	2.5
4	100	100	2	0.2	0.3	0.5	0.5	*	*	4802	13295	20169	5011	12922	20377	-4.3	2.8	-1.0
5	100	0	2	0.2	0.3	0.5	0.5	*	*	3589	12207	18787	3638	11927	18505	-1.4	2.3	1.5
6	5	5	2	0.2	0.3	0.5	0.5	*	*	3779	11743	18762	3808	11574	18919	-0.8	1.4	-0.8
7	100	100	3	0.2	0.3	0.5	0.5	0.7	0.3	4802	13061	18244	5055	12868	18462	-5.3	1.5	-1.2
8	100	0	3	0.2	0.3	0.5	0.5	0.7	0.3	3585	10761	17281	3726	10215	17256	-3.9	5.1	0.1
9	5	5	3	0.2	0.3	0.5	0.5	0.7	0.3	3830	11185	16732	3974	11094	17497	-3.7	0.8	-4.6

It is shown in Table 3 and 4, by increasing in the number of cracks or torsional stiffness in two supports, the accuracy of the frequencies is reduced when errors are acceptable.

4.2. Changing Values of Test Mass and Accuracy of Method

Since the effect of the test mass is considered in Equation 43, this parameter is examined by the following formulation.

$$Ef=\frac{m^*}{M^*}=(\frac{\omega_{wm}}{\omega})^2-1 \quad (43)$$

Table 5. Comparison of the effect of concentrating mass on the frequencies produced by the Timoshenko beam theory with finite element models for different values and positions of mass test

$$\left(\frac{L}{H}=10,K_L=K_R=100\frac{EI}{L},e_1=0.35,e_2=0.5,e_3=0.65,\eta_1=\eta_3=0.35,\eta_2=0.5\right)$$

No.	$\frac{l_m}{L}$	mp	FEM			TBM			Error (%)		
			Ef_1	Ef_2	Ef_3	Ef_1	Ef_2	Ef_3	Ef_1	Ef_2	Ef_3
1	0.1	1	0.05	0.27	3.01	0.01	0.03	3.51	-75.01	-90.18	16.73
2	0.1	2	0.10	0.55	1.36	0.02	0.05	4.02	-73.76	-90.28	194.60
3	0.1	5	0.24	1.42	3.64	0.04	0.13	5.52	-82.03	-90.57	51.98

4	0.1	10	0.48	2.98	8.05	0.12	0.27	8.04	-74.07	-91.02	-0.14
5	0.2	1	0.38	1.38	1.85	0.26	0.20	1.12	-31.31	-85.65	-39.30
6	0.2	2	0.77	2.81	2.97	0.52	0.40	2.25	-31.53	-85.86	-24.21
7	0.2	5	1.93	7.16	8.99	1.31	0.99	5.62	-32.12	-86.13	-37.41
8	0.2	10	3.93	14.81	16.97	2.62	1.99	11.25	-33.29	-86.59	-33.74
9	0.45	1	2.46	0.30	1.37	1.26	0.07	4.16	-48.68	-75.86	202.56
10	0.45	2	4.93	0.59	2.71	2.52	0.14	5.30	-48.85	-75.46	95.92
11	0.45	5	12.40	1.41	6.48	6.31	0.36	8.74	-49.09	-74.37	34.98
12	0.45	10	24.94	2.61	12.04	12.62	0.72	14.48	-49.40	-72.27	20.25

Where *mp* is the percentage of mass ratio.

The obtained parameter from equation 43 that shows the effect of the test mass, has high amount of errors, so it is necessary to modify these amount for solving the inverse problem.

4.3. Effect of Different Length to Height Ratio

In this section, the responses are evaluated with significant changes in the ratio of length to height. Additionally, in the Table 6, the obtained responses from the mother equation and in Table 7, the responses from equation 39 are examined.

Table 6. Comparison between the natural frequencies of the analytical models and finite element models for different ratios of length to height, according to the mother equation ($K_L = K_R = 2.73 \times 10^6, e_1 = 0.5, \eta = 0.5$)

$\frac{L}{H}$	FEM			TBM			Error (%)		
	F1	F2	F3	F1	F2	F3	F1	F2	F3
20	459.4	1335.7	2364.7	477.1	1423.1	2464.2	-3.85	-6.54	-4.21
16	718.45	2094	3608	729.4	2195.9	3715.4	-1.52	-4.87	-2.98
12	1222	3533	5928.7	1254.4	3808.9	6226.6	-2.65	-7.81	-5.03
8	2494.6	7151.8	11394	2666.0	8071.0	12463.8	-6.87	-12.85	-9.39
7	3153.3	8851.9	13856.1	3408.38	10244.3	15492.7	-8.09	-15.73	-11.81
6	4118.7	11350.4	16746.4	4518.8	13400.0	19751.0	-9.72	-18.06	-17.94
5	5388	14598.2	20026.5	6296.1	18224.5	25962.2	-16.85	-24.84	-29.64
4	6807.1	17946.2	26856.1	9432.1	26130.6	35251.2	-38.56	-45.61	-31.26

According to Table 6, it is concluded that obtaining responses in cases where the length to height ratio is less than 12, is faced to many difficulties. Thus in the next step, only beams with more than 12 of this ratio will be considered. In Table 7, the evaluation of the equation (39) is presented.

Table 7. Comparison of the natural frequencies of the analytical models of the Timoshenko with finite element models for different lengths to heights and constant mass ratios ($K_L = K_R = 2.73 \times 10^6, e_1 = 0.5, \eta_1 = 0.5, m = 30.7\ gr, \frac{l_m}{L} = 0.2$)

$\frac{L}{H}$	FEM			TBM			Error (%)		
	F1	F2	F3	F1	F2	F3	F1	F2	F3
20	467.3	1340.6	2354.5	467.5	1360.8	2283.7	-0.05	-1.51	3.01
16	710.6	2006.1	3602.0	710.2	2082.1	3589.5	0.06	-3.79	0.35
12	1211.9	3416.7	5708.7	1204.1	3504.4	5911.7	0.64	-2.57	-3.56
8	2940.7	6787.0	10794.2	2875.5	7048.8	10706.8	2.22	-3.86	0.81

5. Identify Sources of Errors

As one of the main parts of the inverse solution is the use of equation 39 and according to Table 5, it is needed to modify the effect of the test mass. To find the proper parameters for the modification function, the sources of errors should be determined, as given below:

a) The accuracy of the responses is reduced by increasing the mass of concentrated test mass, it is shown in Figure 7.

b) According to Section 3, to model torsional springs in supports, a new method is suggested. Although moment absorption of the suggested numerical model and the analytical model are the same, but longitudinal deformation of nodes in supports are different as shown in Figure 8. This is because the discrepancy of natural frequencies of these two models can be vary slightly. In other words, in analytical models it is assumed that the plane cross-sections remain plane but it is not according to the suggested numerical model.

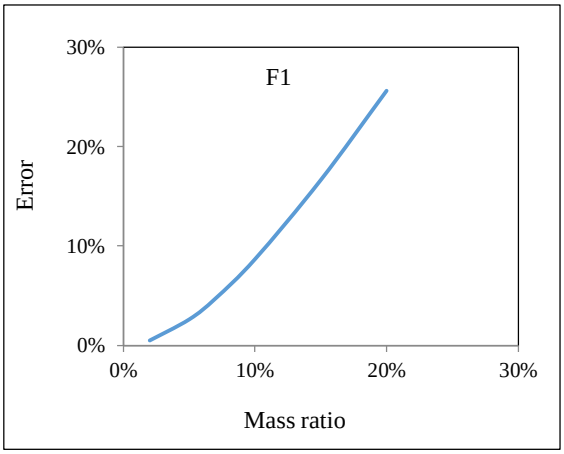

Figure 7. An error in the direct solving of a beam in which the test mass only changes

$$\left(\frac{L}{H}=5, K_L=K_R=0, e_1=0.35, \eta_1=0.5, \frac{l_m}{L}=0.2\right)$$

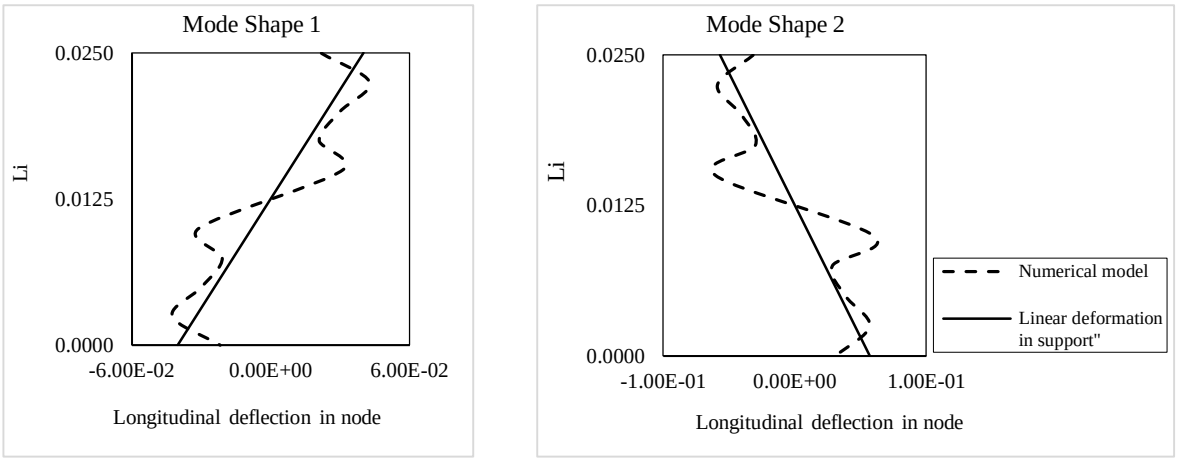

Figure 8. Items show the difference between the deformations of the supports, from fitted function (step d of section 3.2) and the numerical model. The deflections are in the direction of longitudinal springs- ($L_i = l_i + 0.0125$).

These graphs are plotted according to the characteristics of the beam in Table 1, while linear deformation is based on analytical model. The comparison in Figure 8 is based on the mode shapes of the numerical model.

c) Other source of the error is corresponding to the torsional spring that is employed in crack location to show the effect of cracks. It is located in middle of the beam cross-section but it is clearly not true. This amount is significantly less than the other errors, and it is negligible.

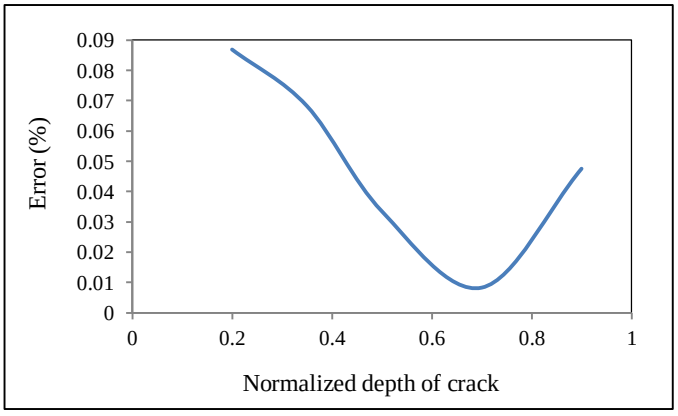

Figure 9. The error in a direct solution, which only the depth of the crack is changed (frequency of the first mode)

$$\left(\frac{L}{H}=5, K_L=K_R=0, e_1=0.35, \eta_1=0.5, \frac{l_m}{L}=0.2\right)$$

Now, in regards to the issues raised in the next section, we consider the functional definition for the correction of the values of the responses obtained in relation to Equation 39.

6. Modification Function

Decision of this section is to find a function that matches the values of numerical and analytical solution. For this purpose, the point-to-point correction coefficient is defined as follows:

$$\frac{M^*}{M^* + ce \times m^*}\omega_{wm}^2 = \omega^2 \tag{44}$$

Where ce is the correction factor for solving the problem that is applied to term of test mass, because solution procedure is based on frequency changes due to the concentrated test mass. Now, to find a relation for this correction parameter Equation 45 is presented which is a function of numerical and analytical frequencies.

$$ce = \frac{\frac{\omega_{wm}^2}{\omega_{numerical}^2} - 1}{\frac{\omega_{wm}^2}{\omega_{analytical}^2} - 1} \tag{45}$$

In general, the effect of test mass is a function of location and amount of itself. Thus, the modification function can be defined by these two parameters and if the location of test mass be fixed, according to Figure 10 to 12 the first or second order function of this mass ratio can be fitted with the point-to-point correction coefficient (ce), this function is named FP.

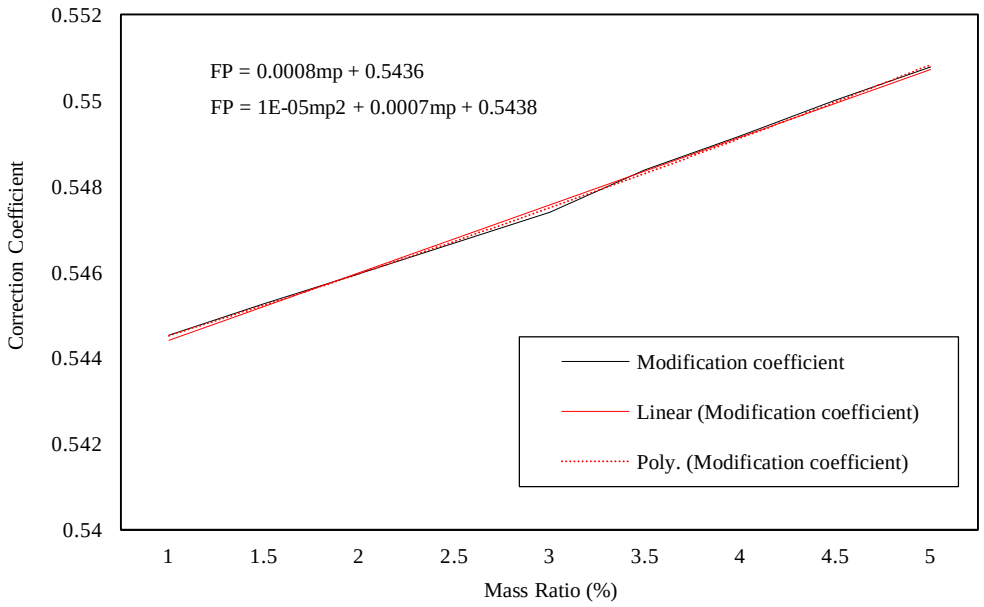

Figure 10. Comparison between linear and the second order correction function

$$\left(\frac{L}{H} = 20, K_L = K_R = 100\,(\frac{EI}{L}), e_1 = 0.35, \eta_1 = 0.5, \frac{l_m}{L} = 0.2\right)$$

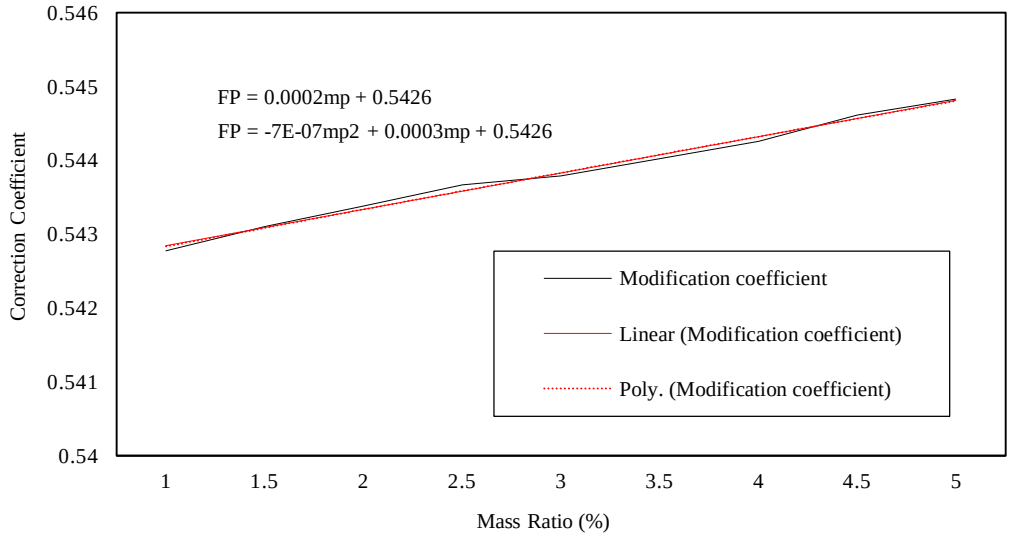

Figure 11. Comparison between linear and the second order correction function

$$\left(\frac{L}{H}=20, K_L=K_R=25\,(\frac{EI}{L}), e_1=0.35, \eta_1=0.5, \frac{l_m}{L}=0.2\right)$$

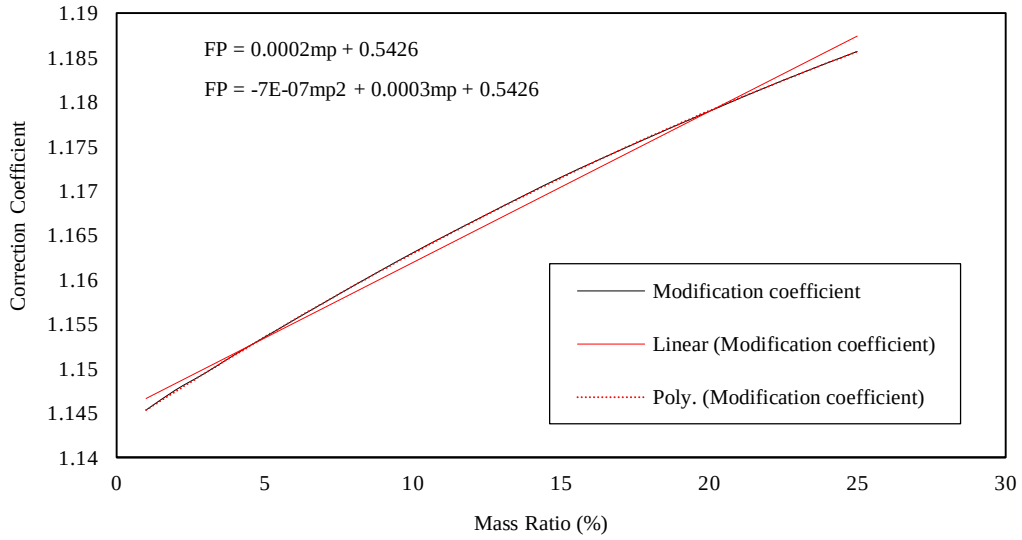

Figure 12. Comparison between linear and the second order correction function

$$\left(\frac{L}{H}=8, K_L=K_R=100, e_1=0.2, e_2=0.5, \eta_{1,2}=0.5, \frac{l_m}{L}=0.375\right)$$

Considering Figure 10 to 12 both of linear and second order correction function (Poly) is acceptable for this problem so correction function is suggested in Equations 46 and 47 where α_i is unknown and should be calculated in solving procedure of inverse solution. This Function is introduced for a test mass that is in a fixed location and the only variable is amount of the test mass. So new correction function should be calculated for different position of the test mass.

$$EQ_i = \frac{M}{M + FP(mp_i)\times m_i}\omega_{wm}^2 - \omega_i^2 \tag{46}$$

$$FP(mp_i) = \alpha_1 + \alpha_2 mp_i + \alpha_3 mp_i^{\,2} + \ldots \tag{47}$$

7. Solving Inverse Problem

In this section, an algorithm is presented to solve the problem which is used in Equations 26 and 46.

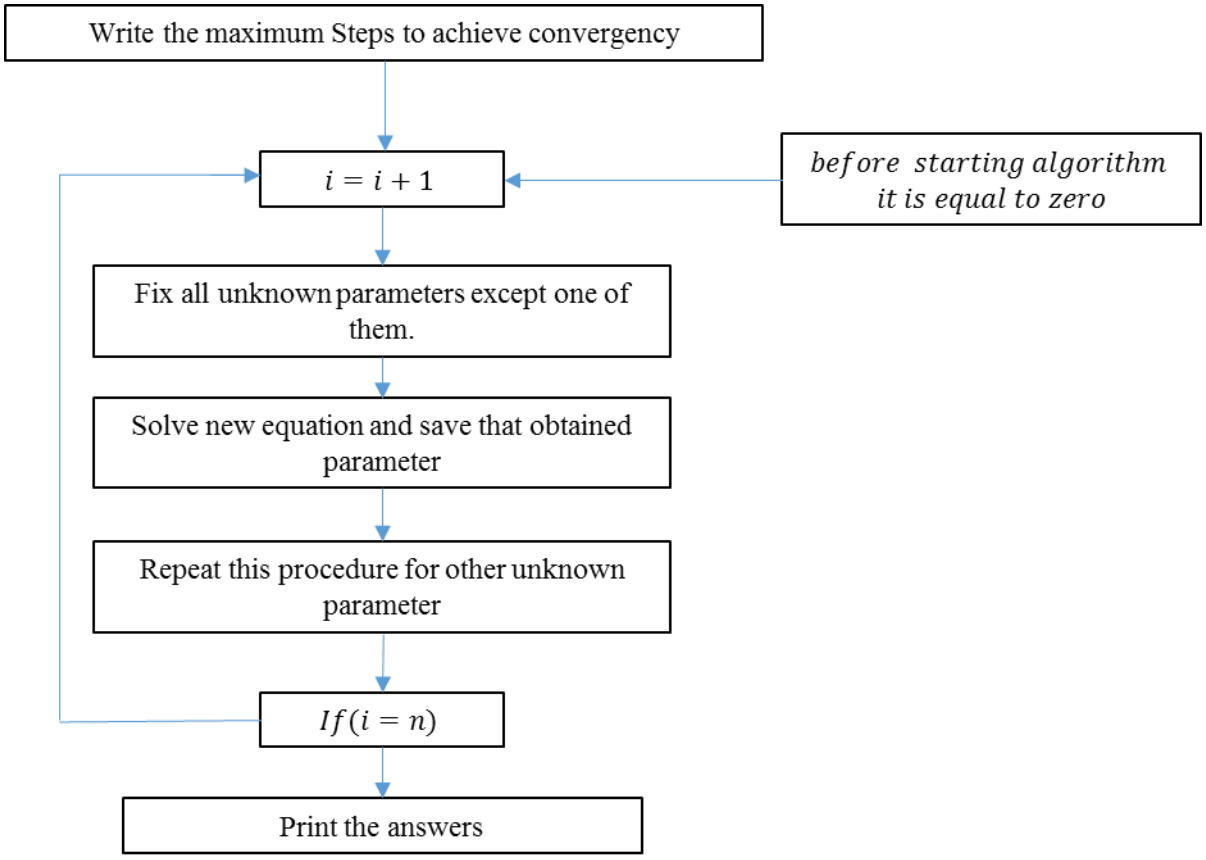

Figure 13. Algorithm of a subroutine that is used in inverse solution algorithm to solve the equation (Figure 14), this is named A + algorithm

Table 8. Inverse solving for a beam with a crack, based on the algorithm that is shown in Figure 14
($K_{L,R}$ is based on the $\frac{EI}{L}$ coefficients.)

The values obtained from the inverse solution				Values Considered in Numerical Models				$\frac{L}{H}$	No.
e_1	η	K_L	K_R	e_1	η	K_L	K_R		
0.75	0.4	0	31.3	0.75	0.4	0	30	12	1

Table 9. The results of the inverse solving of the beam with two cracks according to the algorithm described in Figure 14

The obtained values from the inverse solution						Considered values in Numerical Models						$\frac{L}{H}$	No.
e_2	η_2	e_1	η_1	K_L	K_R	e_2	η_2	e_1	η_1	K_L	K_R		
0.320	0.525	0.201	0.510	0.023	111.0	0.5	0.5	0.2	0.5	0	100	8	1
0.248	0.670	0.500	0.390	9.520	9.940	0.75	0.7	0.5	0.4	10	10	16	2

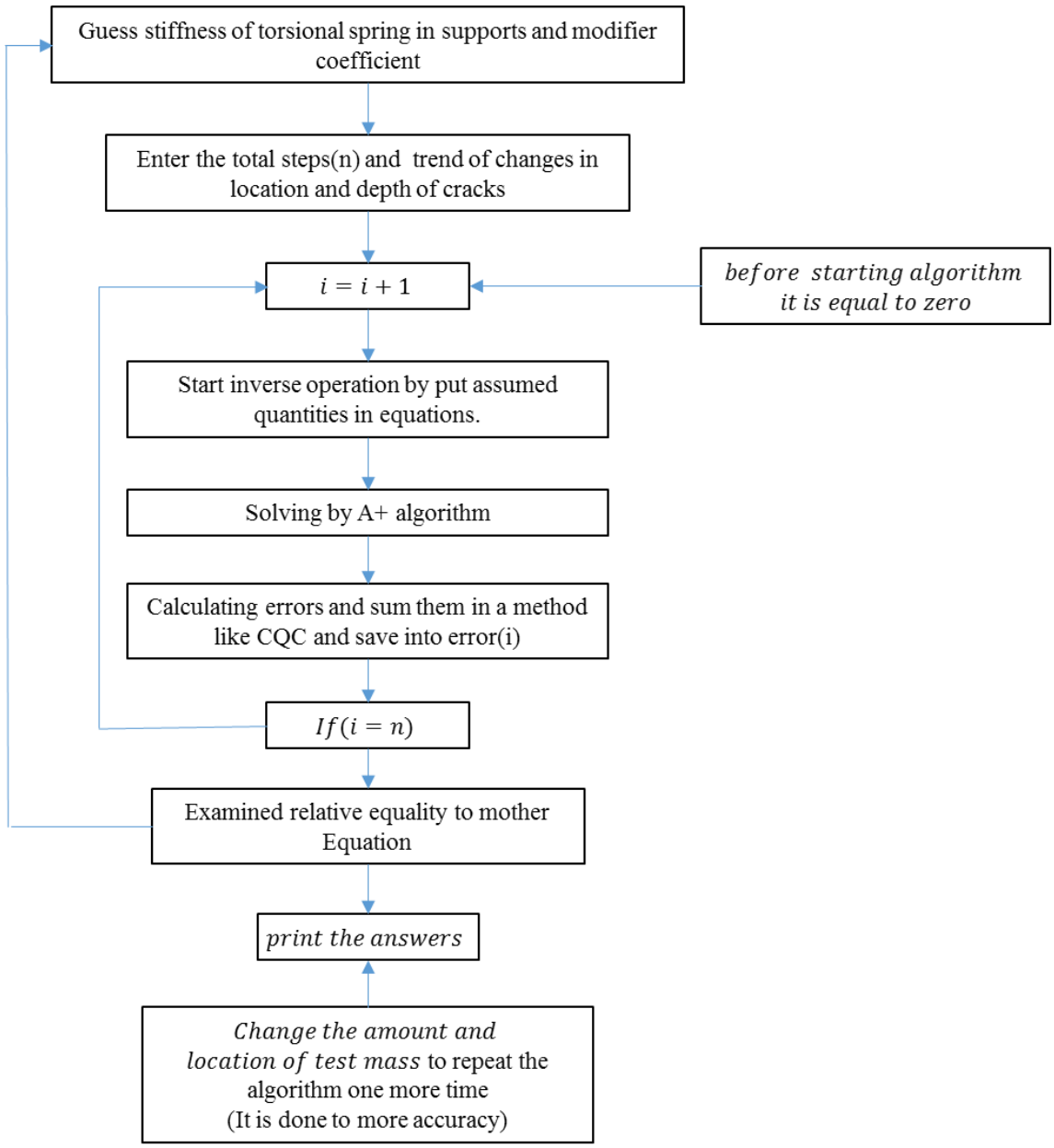

Figure 14. The inverse solution algorithm

1) Regarding the process of variation in Equation 26, variety of frequency by changing in support torsional stiffness is much higher than the other parameter. Therefore, it is possible to guess the support torsional stiffness in the beginning of solving procedure (guess without consideration to cracks).
2) It is possible to guess crack modification function with a reasonable approximation without considering cracks.
3) Given the fact that the parameters of the crack are changed in a certain range, the initial quantity and the range of crack depth should be determined in the algorithm of inverse solving.

According to the above algorithms, the inverse solution is performed and the answers are obtained.

Table 10. The results of inverse solving of the beam with three cracks according to the algorithm shown in Figure 14 ($K_{L,R}$ is based on the $\frac{EI}{L}$ coefficients.)

The values obtained in the inverse solution	Considered values in the Numerical Model	$\frac{L}{H}$=10
197	200	K_L
196	200	K_R
0.310	0.300	η_1
0.520	0.500	η_2
0.280	0.300	η_3
0.340	0.350	e_1
0.152	0.150	e_2
0.160	0.150	e_3

8. Conclusion

In this study, the aim is to reduce the cost of health monitoring of beams, for which the analytical method is used. This procedure contains five main stages. In the first step, equation of cracked beam with one sided open crack and uncertain boundary conditions are presented. In the next stage, a new numerical model is suggested to simulate cracked beam with 2D torsional springs. In the following step, the acceptable performance of the new model is shown. The comparison between responses of numerical and analytical model is performed, and source of errors is identified to solve the inverse problem. A modification coefficient is suggested which is a function of amount and location of the test mass. In the last part, an algorithm for inverse problem is proposed. It is very encouraging that the obtained results of the inverse algorithm are very close to those obtained from the numerical model, when all three aspects of crack detection in a beam is considered.

9. References

[1] Banerjee, Amit, and G. Pohit. "Crack Investigation of Rotating Cantilever Beam by Fractal Dimension Analysis." Procedia Technology 14 (2014): 188-195. DOI: 10.1016/j.protcy.2014.08.025.

[2] S. P. Lele and S. K. Maiti, "Modeling of transverse vibration of short beams for crack detection and measurement of crack extension," Journal of Sound and Vibration, vol. 257, pp. 559–583, 2002. DOI: 10.1006/jsvi.2002.5059.

[3] W. Fan and P. Qiao, "Vibration-based damage identification methods: A review and comparative study," Structural HealthMonitoring, vol. 0, pp. 1–29, Aprill 2010. DOI: 10.1177/1475921710365419.

[4] S. Zhong and S. O. Oyadiji, "Detection of cracks in simply-supported beams by continuous wavelet transform of reconstructed modal data," Computers & Structures, vol. 89, pp. 127-148, 2011. DOI: 10.1016/j.compstruc.2010.08.008.

[5] K. Aydin, "Vibratory Characteristics of Axially-Loaded Timoshenko Beams With Arbitrary Number of Cracks," Journal of Vibration and Acoustics, vol. 129, pp. 341-354, 2007. DOI: 10.1115/1.2731411.

[6] H. Nahvi and M. Jabbari, "Crack detection in beams using experimental modal data and finite element model," International Journal of Mechanical Sciences, vol. 47, pp. 1477-1497 ,2005. DOI: 10.1016/j.ijmecsci.2005.06.008.

[7] P. N. Saavedra and L. A. Cuitino, "Crack detection and vibration behavior of cracked beams," Computers and Structures, vol. 79, pp. 1451–1459, 2001. DOI: 10.1016/S0045-7949(01)00049-9.

[8] U. Andreaus and P. Baragatti, "Cracked beam identification by numerically analysing the nonlinear behaviour of the harmonically forced response," Journal of Sound and Vibration, vol. 330, pp. 721-742, 2011. DOI: 10.1016/j.jsv.2010.08.032.

[9] Wang, Le, and Zhichun Yang. "Identification of boundary conditions of tapered beam-like structures using static flexibility measurements." Mechanical Systems and Signal Processing 25, no. 7 (2011): 2484-2500. DOI: 10.1016/j.ymssp.2011.04.003.

[10] Zhu, X. Q., and Siu-Seong Law. "Structural health monitoring based on vehicle-bridge interaction: accomplishments and challenges." Advances in Structural Engineering 18.12 (2015): 1999-2015. DOI: 10.1260/1369-4332.18.12.1999.

[11] M. Shafiei and N. Khaji, "Analytical solutions for free and forced vibrations of a multiple cracked Timoshenko beam subject to a concentrated moving load," Acta Mechanica, pp. 1-19, 2011. DOI: 10.1007/s00707-011-0495.

[12] He, Wen-Yu, Wei-Xin Ren, and Songye Zhu. "Damage detection of beam structures using quasi-static moving load induced displacement response." Engineering Structures 145 (2017): 70-82. DOI: 10.1016/j.engstruct.2017.05.009.

[13] Lin, Hai-Ping. "Direct and inverse methods on free vibration analysis of simply supported beams with a crack." Engineering structures 26.4 (2004): 427-436. DOI: 10.1016/j.engstruct.2003.10.014.

[14] N. Khaji, M. Shafiei, and M. Jalalpour, "Closed-form solutions for crack detection problem of Timoshenko beams with various boundary conditions," International Journal of Mechanical Sciences, vol. 51, pp. 667-681, 2009. DOI: 10.1016/j.ijmecsci.2009.07.-004.

[15] S. Timoshenko, D. Young, and W. Weaver, Vibration problems in engineering. New York: Wiley, 1974. DOI: 10.1177/058310247500700909.

[16] R. Clough and J. Penzien, Dynamics of Structures (third Edition). Berkley, California: Computers and Structures, Inc, 2003. DOI: 10.1201/b11772.

[17] O. C. Zienkiewicz and R. L. Taylor, The finite element method for solid and structural mechanics: Elsevier Butterworth-Heinemann, 2006. DOI: 10.1061/(asce)0733-9399(2006)132:12(1400).

[18] U. Pabst and P. Hagedorn, "Identification of boundary conditions as a part of model correction," Journal of Sound and Vibration, vol. 182, pp. 565-575, 1995. DOI: 10.1006/jsvi.1995.0217.

[19] K. Aydin, "Vibratory Characteristics of Axially-Loaded Timoshenko Beams With Arbitrary Number of Cracks," Journal of Vibration and Acoustics, vol. 129, pp. 341-354, 2007. DOI: 10.1115/1.2731411.

[20] Nasiri, Sara, Mohammad Reza Khosravani, and Kerstin Weinberg. "Fracture mechanics and mechanical fault detection by artificial intelligence methods: A review."Engineering Failure Analysis 81 (2017): 270-293. DOI: 10.1016/j.engfailanal.2017.07.011.

[21] Greco, A., et al. "Closed-form solution based Genetic Algorithm Software: Application to multiple cracks detection on beam structures by static tests." Applied Soft Computing64 (2018): 35-48. DOI: 10.1016/j.asoc.2017.11.040.

[22] Fekrazadeh, S., and N. Khaji. "An analytical method for crack detection of Timoshenko beams with multiple open cracks using a test mass." European Journal of Environmental and Civil Engineering 21.1 (2017): 24-41. DOI: 10.1080/19648189.2015.1090929.